NASA Contractor Report 4148

Development Program for 1.93-μm Lasers

P. Longeway, T. Zamerowski,
R. Martinelli, R. Stolzenberger,
and N. DiGiuseppe

CONTRACT NAS1-17351
MAY 1988

NASA

NASA Contractor Report 4148

Development Program for 1.93-μm Lasers

P. Longeway, T. Zamerowski,
R. Martinelli, R. Stolzenberger,
and N. DiGiuseppe
David Sarnoff Research Center
Princeton, New Jersey

Prepared for
Langley Research Center
under Contract NAS1-17351

National Aeronautics
and Space Administration

**Scientific and Technical
Information Division**

1988

EXECUTIVE SUMMARY

For the first time, to our knowledge, we have demonstrated lasers operating at 1.93 μm. They were fabricated by Vapor Phase Epitaxial (VPE) growth techniques currently used for the fabrication of high power lasers at 1.3 μm. The structure of these laser diodes consisted of compositionally graded, sulfur-doped InAsP, grown on an InP substrate; a constant-composition n+ $InAs_{0.27}P_{0.73}$ layer, which is the first cladding layer; an $In_{0.66}Ga_{0.34}As$ layer, which is the active region, and a second $InAs_{0.27}P_{0.73}$ layer. The devices were oxide-stripe DH lasers (gain-guided only).

The best devices had 80-K lasing thresholds in the range of from 80 to 150 mA, and T_0 (below 220 K) in the range of 60 to 90 K. The highest observed temperature of oscillation was 15.5°C. The highest observed power output at 80 K was in the range of from 3 to 5 mW. The calculated value for $\Delta\lambda/\Delta T$ was 4.4 Å/K.

As a part of the materials development, we also fabricated PIN homojunction detectors having the bandedge near 1.93 μm. These devices were composed of sulfur-doped graded InGaAs, graded from the composition that is lattice-matched with InP ($In_{0.53}Ga_{0.47}As$), followed by a constant composition region having the bandedge near 1.93 μm ($In_{0.66}Ga_{0.34}As$). The top 0.5 μm of this layer was zinc-doped to establish the p-n junction and for contacting purposes. The best devices (100-μm diameter, mesa structure) exhibited room-temperature dark currents in the range of from 20 to 50 nA and had QE at 1.93 μm in the range of 35 to 40%.

In addition to the device results, the InGaAs-InAsP materials system has been extensively investigated and low defect density layers can now be grown allowing for significant device performance improvement.

A. INTRODUCTION

The tasks encompassed by this contract to develop laser diodes operating at 1.93 μm can be outlined as follows:

Task 1. Choose the materials configuration to be used in the laser fabrication.

Two systems were presented in the technical proposal, as shown in Figs. 1 and 2. The first system consisted of compositionally graded InGaAs grown on an InP substrate, followed by a first n-type InAsP cladding layer, the InGaAs active region, the second p-type InAsP cladding layer, and an InGaAs capping layer. The second configuration consisted of a layer of compositionally graded InAsP grown on an InP substrate, which layer also acts as the first n-type cladding layer; the InGaAs active region; the second p-type InAsP cladding layer; and an InGaAs capping layer.

Task 2. Develop the growth techniques for low defect density graded materials (either InGaAs or InAsP).

This research included evaluation of two different, compositional grading schemes. The first was continuous-grading, in which reactive gas flows were changed with time in a smooth analog fashion with time to produce a continuous, compositional gradient. The second was step-grading, in which the reactive gas flows were changed with time in an abrupt digital fashion to produce a compositionally stepped gradient. An additional issue that had to be evaluated for the step-grading scheme was the number and magnitude of compositional steps to be used.

A second aspect of this research was the effect of dopants, specifically sulfur (n-type), on the defect density of the graded materials.

Task 3. Develop the optimal configuration for the final device structure.

This research included examining the effects of variations in the active-layer thickness, the p-side and n-side doping levels, and the position of the p-n junction with respect to the active layer.

Task 4. Fabrication and evaluation of sources.

This task was closely coupled with Task 3. The devices were evaluated in terms of output, T_o; spectral shift as a function of operating temperature, I_{th}; and emission wavelength.

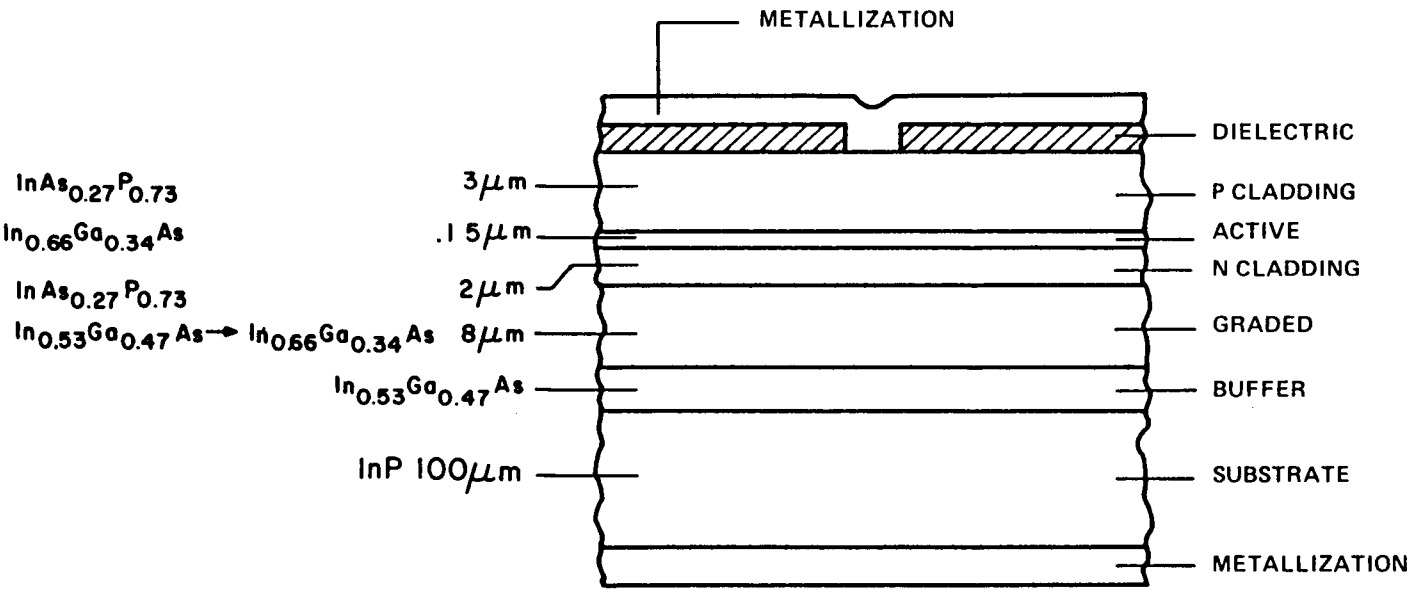

Figure 1. Structure of a 1.93-μm oxide-stripe laser utilizing graded InGaAs as the supporting layer for the n-type InAsP cladding layer.

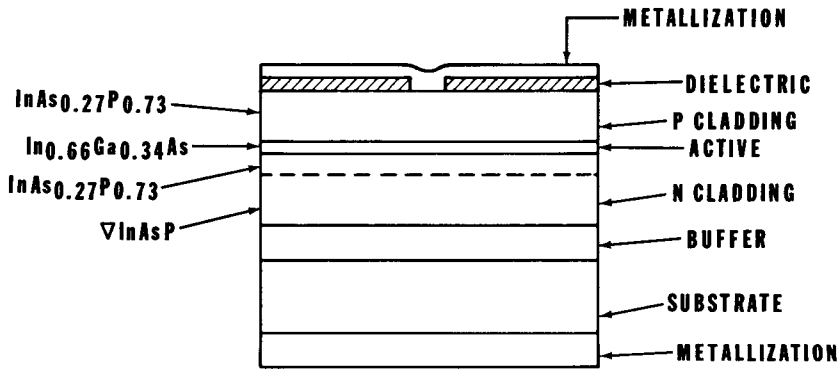

Figure 2. Structure of a 1.93-μm oxide-stripe laser utilizing graded InAsP as the supporting layer for the n-type InAsP cladding layer. This structure has one less heterointerface than its counterpart in Fig. 1.

Additionally, we evaluated the effects of variations in the oxide-stripe width on the device performance.

The following sections of this report outline our approaches and findings regarding these four tasks.

B. MATERIALS CONFIGURATION FOR LASER STRUCTURE

Two material configurations were investigated during the period of this contract. Figure 1 shows the first configuration, which consisted of graded InGaAs grown on an InP substrate as the starting layer, followed by a layer of InAsP lattice matched to the surface of the graded InGaAs layer, which acted as the first cladding layer. Figure 2 shows the second configuration, which consisted of graded InAsP grown on an InP substrate, graded to the appropriate lattice conditions at the surface, then grown as the constant-composition cladding layer.

The graded InAsP structure was more appealing because the structure has one less hetero-interface than that using graded InGaAs. Because these interfaces are locations in the structure where large defect densities can occur, we felt that the graded InAsP structure would yield the best devices. This proved to be true, and the best laser devices we measured came from graded InAsP Samples #8376, #8398, and #8399. Nonetheless, problems were encountered with the growth of the InAsP early in the program.

The first problem was the extremely disproportionate growth rates for the two binaries, InAs and InP, which compose the material. The InAs was observed to grow at a much higher rate than the InP (see Fig. 3), and the fact that the composition of the layer at the InP substrate interface required close to 0% InAs created difficulties. An additional problem was that the morphology of these InAsP graded layers was poor. The surface of the graded layers exhibited large densities of hillocks that made subsequent layer growth difficult. This effect may be caused by the larger compositional variation required in the InAsP (from $InAs_{0.00}P_{1.00}$ to $InAs_{0.27}P_{0.73}$) to bring the lattice parameter of the material to that of InGaAs having a bandgap of 1.93 μm. The compositional variation required for a similar layer of graded InGaAs is from $In_{0.53}Ga_{0.47}As$ to $In_{0.66}Ga_{0.34}As$.

We therefore decided to grow laser devices, using both materials configurations to determine whether the improved morphology of the graded InGaAs materials outweighed the disadvantage of having an extra hetero-interface. This has proved not to be the case. The samples using the graded InAsP materials configuration had lower lasing thresholds at all

operating temperatures, higher values of T_0 and higher maximum temperatures of oscillation than did their graded InGaAs counterparts. We therefore conclude that the graded InAsP materials configuration is the better choice for the laser structure and can be improved even more with optimization of the growth parameters (e.g., growth temperature).

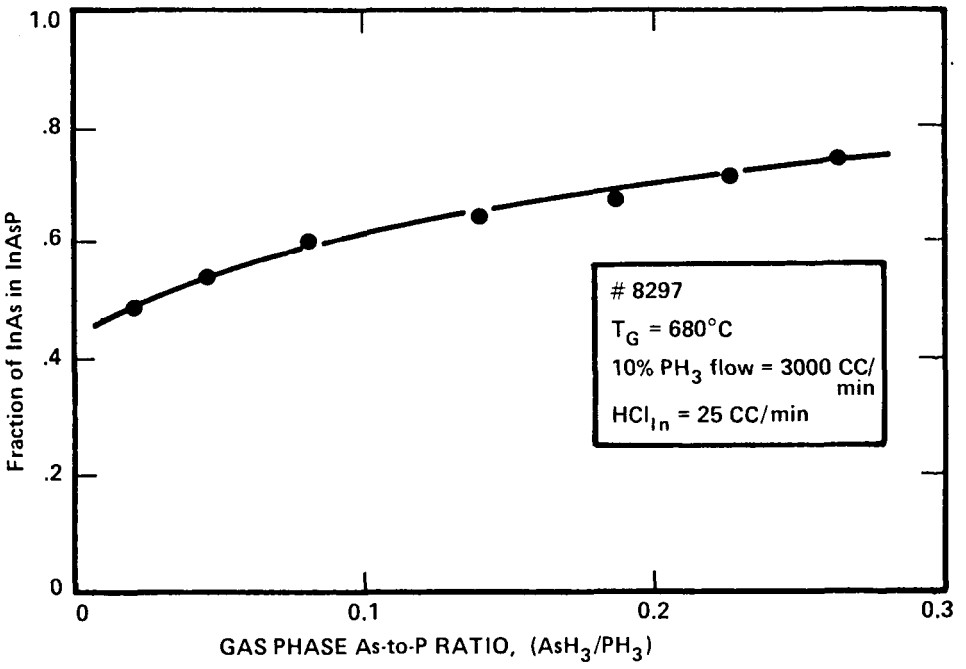

Figure 3. Fraction of InAs appearing in InAsP as a function of the gas phase ratio of the reactant gases AsH_3 to PH_3. The non-zero intercept demonstrates that the 0 flow setting on the AsH_3 flowmeter is not 0 flow and the formation of InAs on the growing surface is more efficient than the formation of InP.

C. DEVELOPMENT OF GROWTH TECHNIQUES FOR LOW DEFECT DENSITY MATERIALS

The growth of compositionally graded ternaries results in lattice parameter grading as well. This condition gives rise to strain in the lattice, which is relieved by the generation of misfit dislocations.[1] The ends of segmental dislocations within the crystal propagate along the axis normal to the substrate, ultimately appearing at the surface.[2] This type of dislocation is therefore called a threading dislocation. Since these dislocations can act as recombination centers in the material, a high defect

density usually translates into a high dark current for photodetectors[3] or a high I_{th} and low radiative efficiency for lasers. It is therefore necessary to reduce the defect density in the graded material to optimize device performance.

Two issues were addressed in our effort to produce low-defect-density graded material: first, the use of high concentrations of sulfur dopant in the graded region to "tie up" dislocation sites, and second, the choice of grading scheme.

A well known method of producing low-defect-density, n-type InP substrates (less than 1 x $10^3/cm^3$) is to highly dope the InP with sulfur during manufacture. Thus, InP substrates having from 6 to 8 x $10^{16}/cm^3$ sulfur concentrations show etch-pit densities as low as $500/cm^3$. We therefore investigated the effect of using high sulfur-doping levels during growth on the dislocation density in graded materials. Table 1 summarizes our findings.

Table 1. Average Dark Currents of Sulfur-doped and Undoped Photodetector Devices

Sample #	I_d (nA) at -5 V	Sulfur Added
8322-1	35	no
8322-2	85	no
8322-3	160	no
8368-1	15	yes
8368-2	20	yes
8368-3	22	yes

It is clear from these results that high levels of sulfur doping (8 x $10^{18}/cm^3$) in the graded region results in lower dark currents in these photodetectors. This observation is also consistent with the results of TEM analysis of graded layers. As shown in Fig. 4, the visible defect density in the highly sulfur-doped samples is less than that of their undoped counterparts. The lower detection limit of this TEM technique is about 10^5 defects/cm^3.

Figure 4(a). Transmission Electron Microscope photograph of the surface of a non-sulfur-doped graded InGaAs sample. Dislocations appear as short, dark lines in the photograph. The dislocation density is about 1 x 10^8 defects/cm^2.

Figure 4(b). TEM photograph of the surface of a sulfur-doped graded InGaAs sample. No defects are visible within the field of the photograph. The lower detection limit for defects using this technique is about 1 x 10^5 defects/cm^2. The lines appearing in the micrograph are artifacts of the etching procedure.

Seven of the nine fully evaluated, 1.93-μm laser wafers were grown using a step-grading scheme. The graded regions consisted of nine abrupt steps, the average step size being about 0.11 (dA/A) %/μm. The other two samples were continuously graded. Table 2 presents the lasing threshold of devices prepared from these nine wafers. As can be seen from the results, there is no clearcut indication that step-grading is superior to continuous grading. We have folded these findings in with those of other research programs involving growth of graded materials, and the results remain

inconclusive. However, there are indications that the magnitude of the final step from the graded region to the constant-composition region (see Figs. 1 and 2) is important.[4] The performance of photodetectors grown for this and other programs suggests that a relatively large step, about 0.30 (dA/A)%, is preferable in terms of reduced dark current to a smaller final step. This is consistent with the model for dislocation generation discussed earlier in that a larger final step would be more effective in turning over the dislocations. It may be that the grading scheme employed during growth is relatively unimportant provided the final grading step is optimized. Clearly, additional research into these questions is needed.

Table 2. I_{th} (80 K) of Samples Employing Differing Grading Schemes

Sample #	Graded Material	Type of Grading	Grading Rate (dA/A)%/μm	I_{th} (80 K)
8374	InGaAs	Continuous	0.08	215 mA
8375	InGaAs	Continuous	0.10	130 mA
8376	InAsP	Stepped	0.09	80 mA
8387 (n cavity)	InAsP	Stepped	0.11	None
8393 (n cavity)	InAsP	Stepped	0.10	550 mA
8395 (n cavity)	InAsP	Stepped	0.11	2200 mA
8396 (n cavity)	InAsP	Stepped	0.07	1150 mA
8398	InAsP	Stepped	0.09	400 mA
8399	InAsP	Stepped	0.14	150 mA

D. DEVICE CONFIGURATION

Three issues were investigated in our efforts to optimize the device configuration: first, the p- and n-type doping levels on either side of the junction, second, the position of the p-n junction with respect to the cavity, and third, the thickness of the active layer in the device.

Our experience in the fabrication of 1.3- and 1.55-μm oxide-stripe lasers demonstrated to us that the doping profile of these devices should be relatively flat, i.e., the doping level on either side of the junction should be approximately the same. Devices that had a difference in the p- and n-type doping levels on either side of the junction, by a factor of three or better, lased with low output. Following this lead, we adjusted the flow rates of the dopant gases to achieve a relatively flat doping profile. Figure 5 presents the Polaron (C-V) profile of a 1.93-μm device optimized for doping levels.

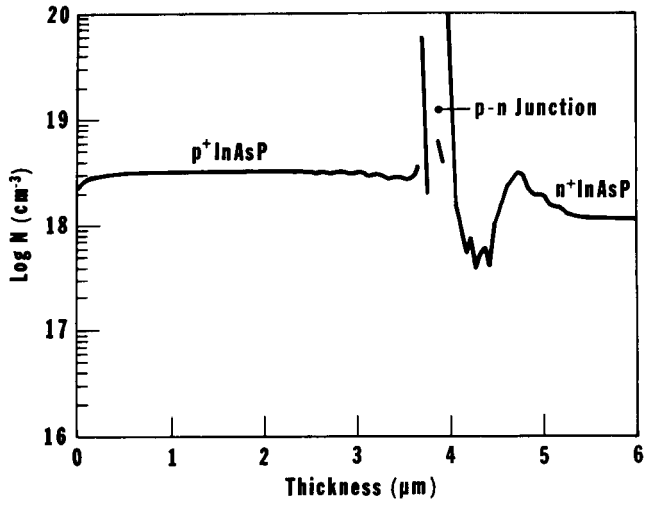

Figure 5. Polaron C-V profile of a 1.93-μm DH laser structure. The dip in the doping level near 4-μm depth indicates that the p-n junction is not fully into the cavity of the structure.

A second and more significant question within this discussion was the dopant type of the cavity, i.e., mostly p-type or mostly n-type. The best 1.3- and 1.55-μm devices fabricated in our laboratories had mostly p-type cavities. By "mostly p-type" we mean that the p-n junction was within the cavity but nearest the n-type cladding layer. Several 1.93 μm samples were grown using this configuration, but we were also interested in the behavior of devices having mostly n-type cavities. Theoretical calculations of the gain to be expected in p- and n-type cavities of III-V laser structures show those with n-type cavities to have almost twice the gain.[5]

In accordance with this, four samples were grown with deliberately n-doped cavities. None of these four samples produced lasing devices

(several behaved as poor LEDs). Subsequent analysis of the position of the p-n junction with respect to the cavity, using EBIC (Electron Beam Induced Current) techniques suggested, not unambiguously, that the junction was in the p-type cladding layer within 0.3 μm of the cavity interface. Figure 6 shows several EBIC traces for different 1.93-μm laser structures. Again, our experience with the 1.3- and 1.55-μm program has taught us that this is not where the p-n junction should be placed. Figure 7 shows the bandgap diagrams of three possible laser configurations: (1) one that has a wholly n-type cavity with the junction outside the cavity, (2) one that has the junction within the cavity, and (3) one that has a wholly p-type cavity with the junction outside the cavity. In the first case (the wholly n-type cavity), holes are injected into the cavity either very inefficiently or not at all. The intermediate case is optimal but extraordinarily difficult to achieve in actual growth practice. The latter case (the wholly p-type cavity) remains efficient due to the much higher injection rate of electrons vs holes.

The thickness of the cavity in a lasing structure must be optimized with respect to the emission wavelength of the device and the confinement characteristics of the chosen cladding layers. Figure 8 presents the theoretical calculation of the confinement factor vs the cavity thickness for 1.93-μm emission. The lowest lasing threshold should occur at a cavity thickness corresponding to the minimum in the curve, which occurs at about 0.40 μm. The cavity thicknesses of our samples varied in the range of from 0.40 to 0.60 μm. No significant differences in device performance were observed for these samples.

E. DEVICE EVALUATION AND PERFORMANCE

In addition to the samples grown for the purposes of materials evaluation, nine laser structures and two detector structures were grown and fully evaluated. A summary of the results for these wafers is listed as Table 3. In the following sections, we discuss our findings with respect to the lasing threshold (I_{th}), the change in lasing threshold with temperature (T_o), the highest temperature of oscillation, and the emission wavelength.

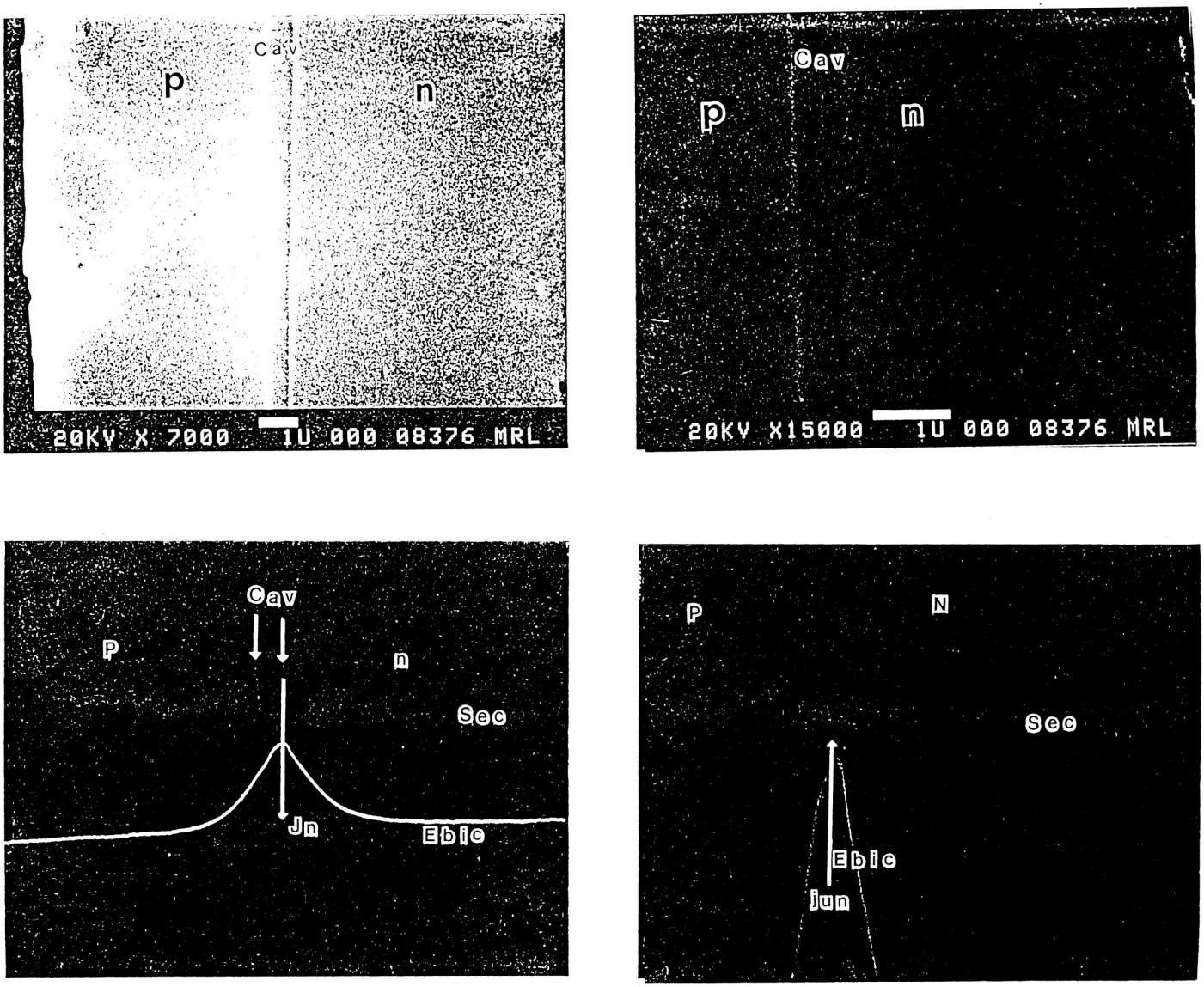

Figure 6. SEM photographs (top) and EBIC traces for two devices from Sample #8376. The position of the cavity is indicated on both the SEM photographs and the EBIC traces. The symmetric shape of the EBIC trace about the peak (the junction) indicates that the p-n junction is properly located and devices prepared from the sample will lase.

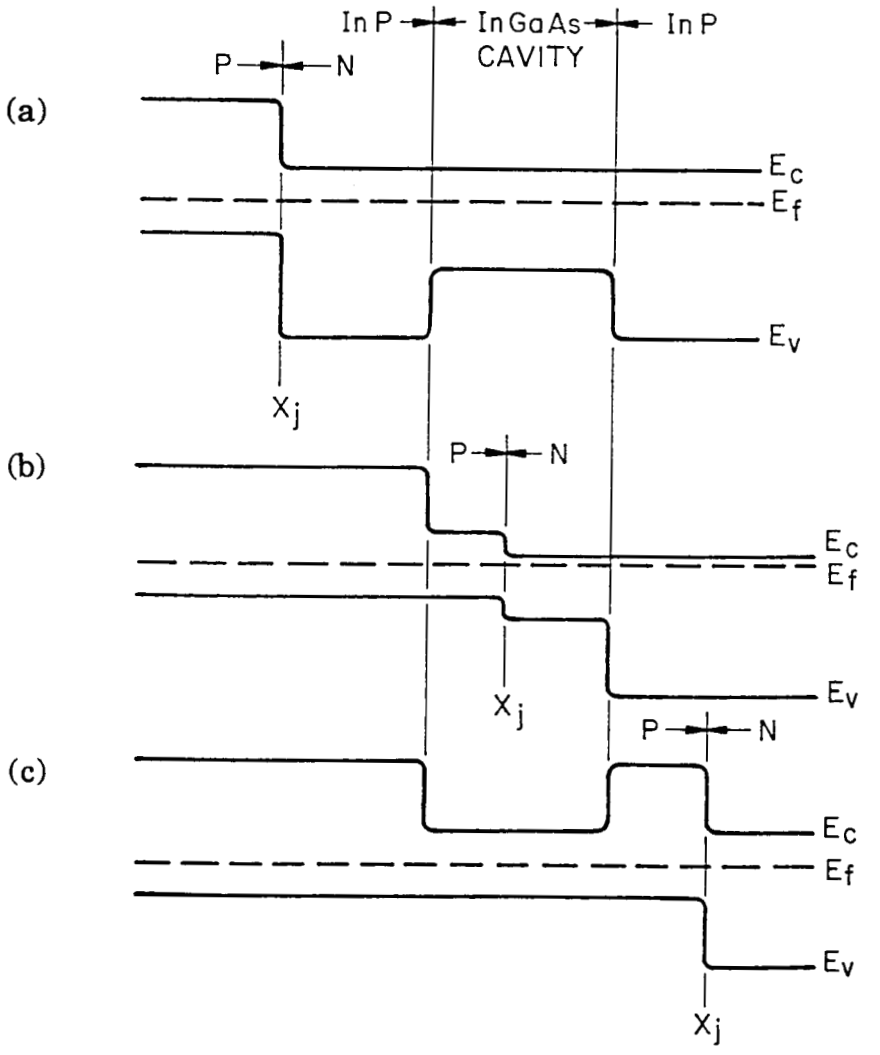

Figure 7. Bandgap diagrams of DH laser structures wherein the p-n junction is located
(a) in the p-cladding layer,
(b) in the cavity, and
(c) in the n-cladding layer.
For case (a), holes must be injected into the cavity from the cladding layer. Since hole mobility and lifetime is much less than for electrons, injection is highly inefficient. For case (b), electrons are injected from the cladding layer, which is more efficient than the case for holes.

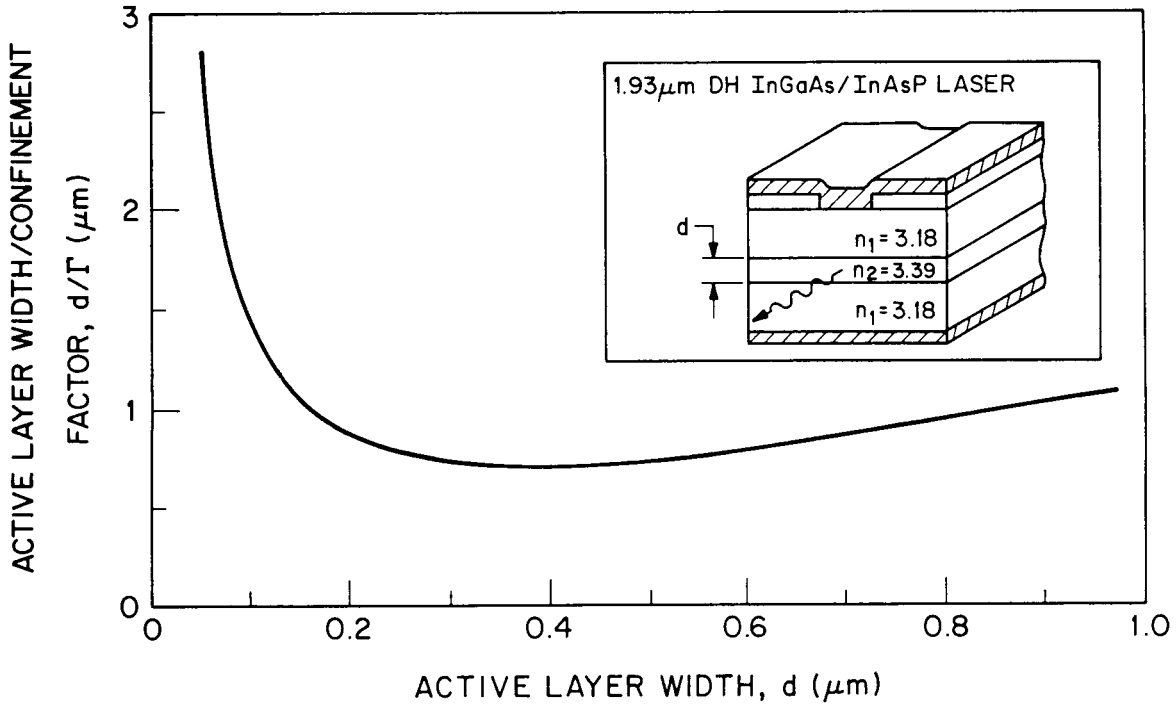

Figure 8. Theoretical calculation of the confinement factor as a function of the cavity width for a 1.93-μm DH laser having an InGaAs active region and InAsP cladding layers. As 1/(confinement factor) is plotted, the minimum in the curve represents the optimal cavity width.

Table 3. Summary of Evaluation of 1.93-μm Lasers

Sample #	I_{th} (mA) 80 K	T_o (K)	Highest T of Oscillation	Wavelength (μm) 80 K	Power Out mW (80 K)
8374	215	---	---	1.90	---
8375	130	73	248	1.88	0.7
8376	80	57	260	1.84	3.0
8387	No observed lasing				
8393	550	84	240	1.71	---
8395	2200	129	180	---	0.5
8396	1150	94	210	---	---
8398	400	103	270	---	2.5
8399	150	86	289	1.86	4.8

The lowest measured lasing threshold at 80 K for our samples was 32 mA. This device came from Sample #8376, which had an average value for I_{th} of 80 mA, based on eight devices. The devices from this sample also demonstrated the lowest value for T_0 (57 K) and one of the highest temperatures at which lasing extinguished (260 K). Figure 9 presents a log-log plot of I_{th} at 80 K vs the highest observed temperature of oscillation. The data suggest that the best chance of achieving room temperature oscillation occurs when the 80 K I_{th} is in the range of from 30 to 50 mA. Sample #8376 demonstrates that lasing thresholds in this range are achievable. Therefore, it is our opinion that room temperature oscillation is also achievable, provided the materials, doping profile, and other structural parameters are optimized.

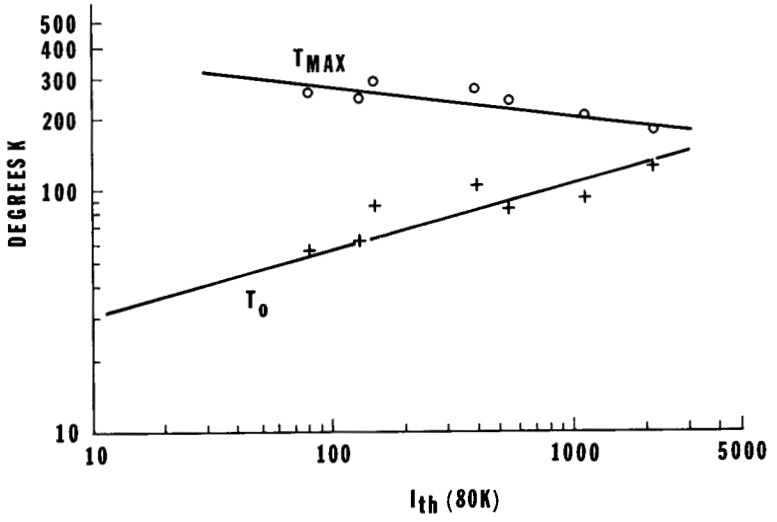

Figure 9. Plots of I_{th} at 80 K vs both T_0 and the maximum temperature of oscillation (T_{max}). While the maximum temperature at which oscillation occurs increases with lower 80 K I_{th}, the value of T_0 decreases, that is, the dependence of I_{th} on T increases.

Figure 9 also presents a plot of the I_{th} at 80 K vs the calculated value of T_0. The data show that, as the 80 K lasing threshold decreases, the value of T_0 falls as well, i.e., the lasing threshold is more sensitive to temperature for the low 80 K threshold devices. The plots of I_{th} vs T for the nine samples listed in Table 3 also show a change in the slope at higher temperatures, i.e., a change in the value of T_0. For seven of the nine samples, this change occurs in the temperature range of from 200 to 220 K, and for eight of the samples, the new slope corresponds to T_0 = 20 to 25 K. Clearly, some new

loss mechanism is becoming dominant in this temperature range and degrading the performance of the devices.[6]

The highest temperature of oscillation observed in these samples was 289 K (16°C) for Sample #8399. While the 80 K lasing threshold for this sample was not the lowest observed, being about 150 mA, the value of T_0 was such that its performance above 200 K was comparable with Sample #8376, which had an 80 K threshold of about 40 mA. Figure 10 presents the least-squares-fitted slopes of I_{th} vs T for four samples. The data points

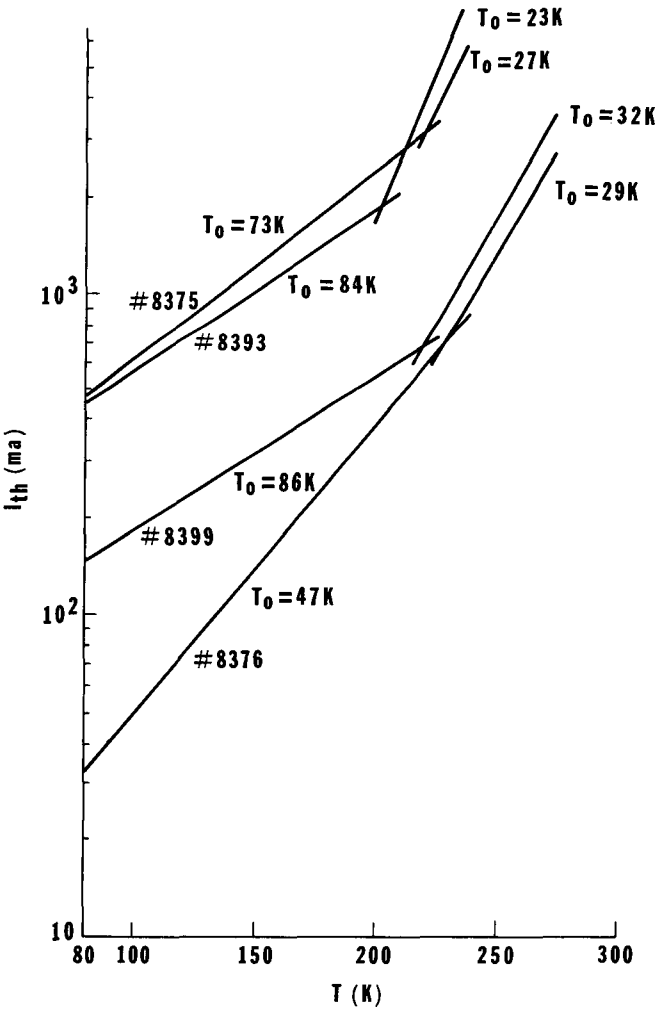

Figure 10. Least-squares fitted curves for the data points of 1 n I_{th} as a function of T (T_0 plots) for four 1.93-μm laser samples. The actual data points have been omitted to prevent clutter. The change in slope for the curves at about 200 to 220 K indicates the onset of an additional loss mechanism for electrons and holes generated within the cavity.

have been omitted to avoid clutter. Thus, at 240 K, for Sample #8376, I_{th} = 1000 mA, and for Sample #8399 at the same temperature, I_{th} = 1300 mA.

The emission wavelength of the device is a function of the composition of the InGaAs in the cavity, the doping level and type of the material in the cavity, and the temperature of operation. It has been our aim to adjust the InGaAs cavity composition for emission at or very near 1.93 μm for room-temperature operation. We therefore measured the emission wavelength of Sample #8375 at various temperatures between 80 K and 150 K. A plot of these results are presented as Fig. 11. The slope of the line is 4.4 Å per degree K. Thus, for room-temperature operation at 1.93 μm, the 80 K emission should fall near 1.83 μm. The issue is further complicated by the fact that, for a given temperature of operation, changes in the drive current of the device result in changes in the dominant mode. Figure 12 presents a plot of the dominant emission peak as a function of the drive current for Sample #8375 operated at 150 K. Thus, to maximize the power output of the device, we must know the dominant mode at room temperature in the range of expected drive currents for the device. Figure 13 presents the emission spectrum for Sample #8399 at 81 K. The strongest longitudinal mode occurs at 1.858 μm. The measured modal spacing is about 26 Å. This is in good agreement with our calculations that the mode spacing is about 21 Å at 1.86 μm. The linewidth in Fig. 13 arises from instrumental resolution, the actual linewidth of the modes being narrower.

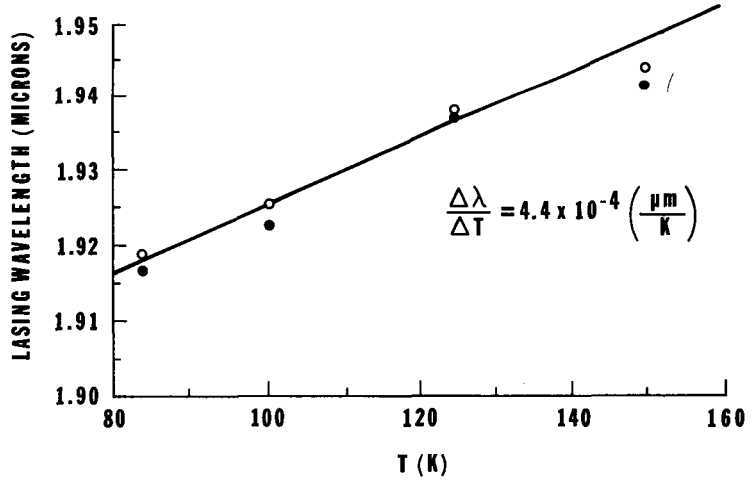

Figure 11. Plot of the wavelength of the dominant longitudinal mode in the emission spectrum of two samples vs the operating temperature. The slope of the least-squares fitted line through the data points has a value of about 4.4 Å/°K.

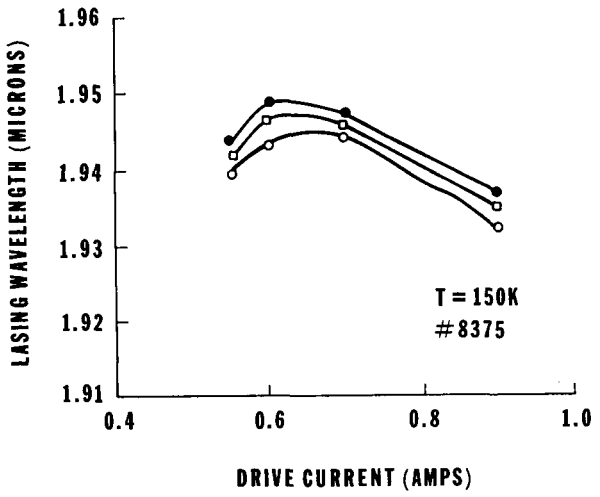

Figure 12. Plot of the wavelength of the three dominant longitudinal modes for Sample #8375 as a function of the drive current (at 150 K).

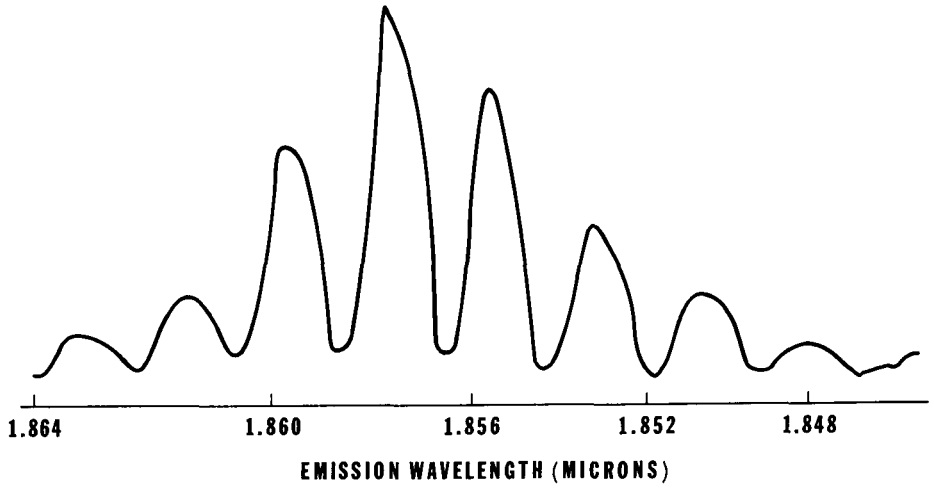

Figure 13. Emission spectrum of sample #8399 operated near threshold at 81 K. The measured spacing between the peaks of the longitudinal modes is 26 Å. The theoretical calculated value is estimated to be 21 Å.

We were able to measure the output of several devices at 80 K, using a PbS detector. This measurement was accomplished by first plotting the detector voltage vs the output of a calibrated 1.55-μm source. The responsivity of the detector was then measured spectrometrically at 1.55 and 1.85 μm and the appropriate conversion factor applied to the detector voltage arising from 1.85-μm illumination. The highest measured output

occurred for Sample #8399 and was in excess of 3 mW at 80 K. Other measured samples fell in the range of from 1.0 to 2.5 mW. Figure 14 presents a typical P-I curve for Sample #8399-M1011.

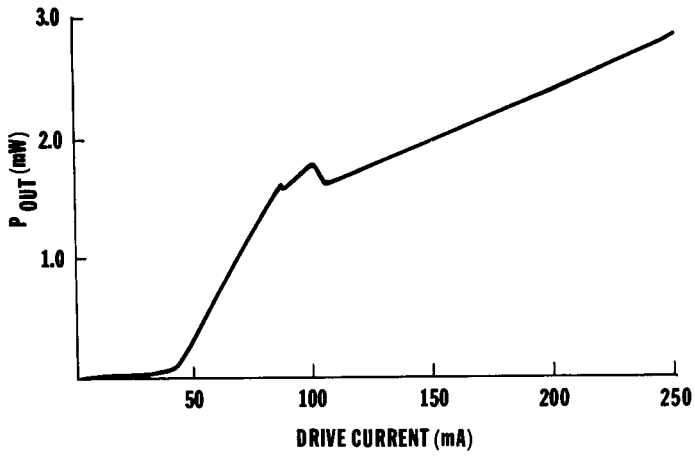

Figure 14. Plot of power output versus drive current at 80 K for Sample #8399-M1011. The values of P_{out} are estimated from the detector response at 1.55-μm for a calibrated 1.55 μm source and the measured relative responsivity of the detector at 1.55 and 1.85 μm.

Although we did not perform an extensive evaluation of the effect of stripe width on the device performance of these oxide-stripe lasers, one sample was processed into both 12.5- and 40-μm stripe devices. The highest temperature of oscillation and the T_0 values for both remained about the same. The 80 K lasing threshold of the 12.5-μm stripe width device was 32 mA; that of the 40-μm-stripe-width device was 80 mA (Sample #8376).

As a part of the materials study, we also prepared two full homojunction PIN photodetectors. The lowest dark currents in these devices were observed for Sample #8368, 40 nA at 295 K. We include as Fig. 15 the responsivity curve for Sample #8322. Calculation of the quantum efficiency at 1.93 μm from this curve, assigns the value as about 32%.

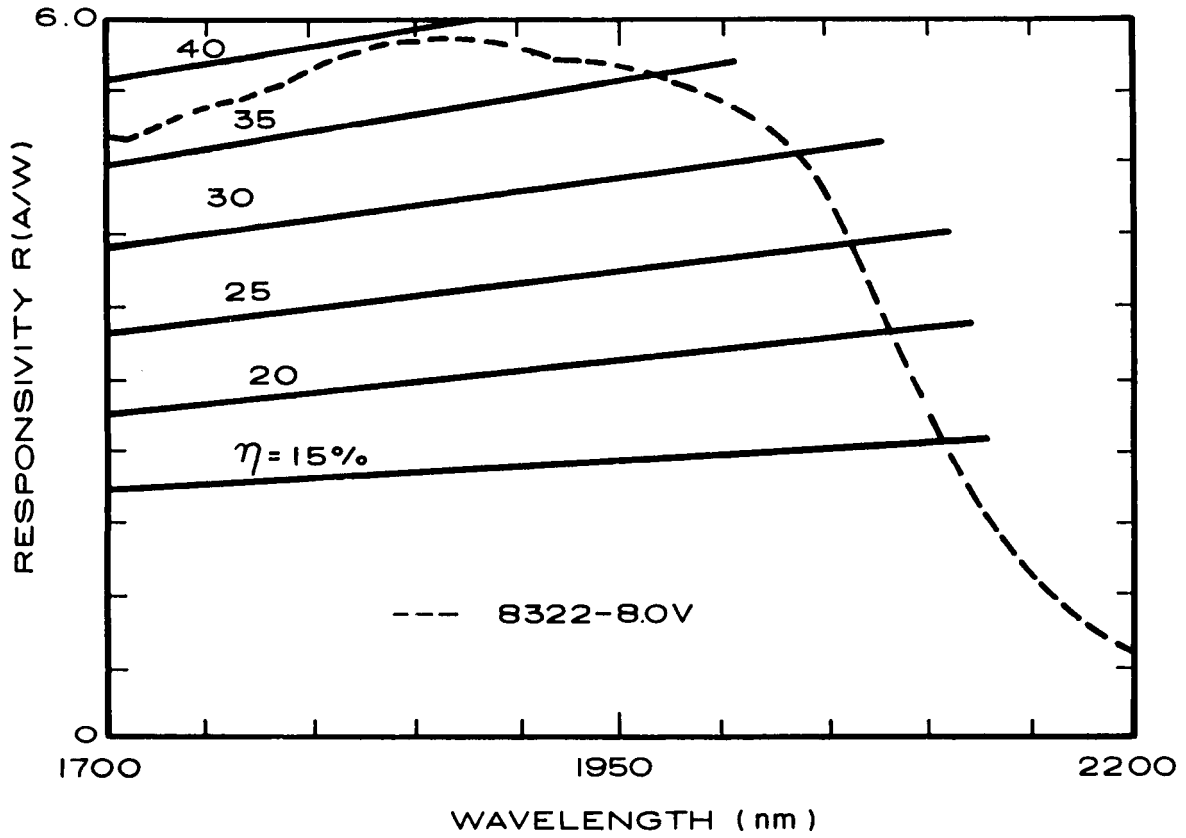

Figure 15. Responsivity of a 1.93-μm detector (Sample #8322) at wavelengths in the range of from 1700 to 2200 nm. Constant QE lines have been superimposed on the graph to indicate the QE at 1.93 μm to be about 37%.

F. SUMMARY OF RESULTS

The InGaAs-InAsP materials system that was chosen for the 1.93-μm laser structure has been extensively investigated. The defect density in the graded material has been reduced to less than 1 x $10^5/cm^{-3}$, using sulfur doping and an appropriate grading scheme. Despite the difficulties with growth, graded InAsP was chosen as the supporting layer for the cladding and active regions because the final structure has one less heterointerface than the graded InGaAs structure, and our results using this materials have been encouraging. Nine laser wafers have been fully processed and evaluated as DH oxide-stripe configurations. Additionally, two detector wafers have been fabricated and evaluated in the homojunction mesa configuration.

The lowest observed lasing threshold at 80 K was 32 mA for Sample #8376, using a 12.5-μm stripe width. The best T_0 value also was measured on this sample; it was 129 K. The highest observed temperature at which oscillation extinguished was 15.5°C, for Sample #8399. Five of the nine laser wafers showed oscillation above 240 K (-23°C). The 80 K emission wavelength for three samples fell in the range of from 1.71 to 1.90 μm, which, from the observed dependency of wavelength vs T, corresponds to room-temperature oscillation in the range of from 1.806 to 1.996 μm. The highest measured output at 80 K occurred for Sample #8399 and was >3 mW. Other samples fell in the range of from 1.0 to 2.5 mW. The lowest measured dark current for the photodetectors at -5 V bias was 40 nA. This sample also had a calculated quantum efficiency of about 35%.

G. FUTURE WORK

Based on the results of this program, it seems evident that room temperature operation of 1.93 μm laser diodes fabricated in the InGaAs/InAsP materials system is feasible. Further research with various grading schedules (stepped, continuous, non-linear, abrupt step, etc.) will allow us to optimize the materials and device structure. Fabrication of index-guided devices, such as ridge guide lasers or buried ridge guide lasers, will further reduce the lasing thresholds and allow operation at higher temperatures.

Further optimization of the materials will also permit the fabrication of PIN photodetectors with QE at 1.93 μm in the range 70-80%. Improvement in the growth of the InAsP material will permit the fabrication of heterojunction PIN detectors, which intrinsically have higher efficiency than their homojunction counterparts due to the higher bandgap capping layer.

REFERENCE LIST

1. G. H. Olsen, "Interfacial Lattice Mismatch Effects in III-V Compounds," J. Crystal Growth, Vol. 31, pp. 223-239 (1975).
2. M. S. Abrahams, L. R. Weisberg, C. J. Buiocchi and J. Blanc, "Dislocation Morphology in Graded Heterojunctions: $GaAs_{1-x}P_x$," Journal of Materials Sciences, Vol. 4, p. 223 (1969).
3. S. Kagawa, J. Komeno, M. Ozeki and T. Kaneda, "Planar $Ga_{0.47}In_{0.53}As$ PIN Photodiodes with Extremely Low Dark Current," OFC '85, San Diego, CA, February 11-13, 1985.
4. G. H. Olsen and T. J. Zamerowski, "Crystal Growth and Properties of Binary, Ternary and Quaternary (In,Ga)(As,P) Alloys Grown by the Hydride Vapor Phase Epitaxy Technique," Prog. Crystal Growth Charact., 1979, Vol. 2, pp. 309-375, Pergamon Press, Ltd., UK.
5. G. P. Agrawal and N. K. Dutta, Long Wavelength Semiconductor Lasers, Van Nostrand Reinhold Co., New York, 1986.
6. L. C. Chiu and A. Yariv, "Auger Recombination in Quantum-Well InGaAsP Heterostructure Lasers," IEEE J. of Quantum Elect., Vol. QE-18, p. 1406 (1982).

NASA
National Aeronautics and Space Administration

Report Documentation Page

1. Report No.	2. Government Accession No.	3. Recipient's Catalog No.
NASA CR-4148		

4. Title and Subtitle

Development Program for 1.93-μm Lasers

5. Report Date
May 1988

6. Performing Organization Code

7. Author(s)

P. Longeway
T. Zamerowski
R. Martinelli
R. Stolzenberger
N. DiGiuseppe

8. Performing Organization Report No.
DSRC-88-CR-1

10. Work Unit No.
506-44-21-01

9. Performing Organization Name and Address

David Sarnoff Research Center
Princeton, NJ 08543-5300

11. Contract or Grant No.
NAS1-17351

13. Type of Report and Period Covered
Contractor Report
9/24/86 through 9/24/87

12. Sponsoring Agency Name and Address

National Aeronautics and Space Administration
Langley Research Center
Hampton, Virginia 23665

14. Sponsoring Agency Code

15. Supplementary Notes

Langley Technical Monitor: Herbert D. Hendricks

16. Abstract

For the first time, to our knowledge, we have demonstrated lasers operating at 1.93 μm. They were fabricated by Vapor Phase Epitaxial (VPE) growth techniques currently used for the fabrication of high power lasers at 1.3 μm. The structure of these laser diodes consisted of compositionally graded, sulfur-doped InAsP, grown on an InP substrate; a constant-composition n+ $InAs_{0.27}P_{0.73}$ layer, which is the first cladding layer; an $In_{0.66}Ga_{0.34}As$ layer, which is the active region, and a second $InAs_{0.27}P_{0.73}$ layer. The devices were oxide-stripe DH lasers (gain-guided only).

The best devices had 80-K lasing thresholds in the range of from 80 to 150 mA, and T_0 (below 220 K) in the range of 60 to 90 K. The highest observed temperature of oscillation was 15.5°C. The highest observed power output at 80 K was in the range of from 3 to 5 mW. The calculated value for $\Delta I/\Delta T$ was 4.4 Å/K.

As a part of the materials development, we also fabricated PIN homojunction detectors having the bandedge near 1.93 μm. These devices were composed of sulfur-doped graded InGaAs, graded from the composition that is lattice-matched with InP ($In_{0.53}Ga_{0.47}As$), followed by a constant composition region having the bandedge near 1.93 μm ($In_{0.66}Ga_{0.34}As$). The top 0.5 μm of this layer was zinc-doped to establish the p-n junction and for contacting purposes. The best devices (100-μm diameter, mesa structure) exhibited room-temperature dark currents in the range of from 20 to 50 nA and had QE at 1.93 μm in the range of 35 to 40%.

In addition to the device results, the InGaAs-InAsP materials system has been extensively investigated and low defect density layers can now be grown allowing for significant device performance improvement.

17. Key Words (Suggested by Author(s))	18. Distribution Statement
long wavelength devices III-V semiconductor devices 1.93 micron devices	Unclassified - Unlimited Subject Category 36

19. Security Classif. (of this report)	20. Security Classif. (of this page)	21. No. of pages	22. Price
Unclassified	Unclassified	23	A02

NASA-Langley, 1988